Distributed Sensory System of Surface Cracks Monitoring Based on Electrical Impedance Tomography

Eugeny A. Ryndin [1],* , Boris G. Konoplev [1] and Irina V. Kulikova [2]

[1] Institute of Nanotechnologies, Electronics and Equipment Engineering, Department of Electronic Apparatuses Design, Southern Federal University, Rostov-on-Don 344006, Russia; kbg@sfedu.ru

[2] JSC "RPC "Istok" named after Shokin", Fryazino 141190, Moscow Region, Russia; cuttlefish99@mail.ru

* Correspondence: rynenator@gmail.com; Tel.: +7-904-507-4041

check for updates

Abstract: In this paper, we propose a method of distributed sensory systems designing for monitoring of surface cracks in highly loaded constructions based on electrical impedance tomography. A thin conductive film with contacts on the perimeter applied on the monitored surface is used as a crack sensor. Registration and monitoring of surface cracks using the developed modified method of electrical impedance tomography (EIT) are carried out. The proposed method differs from the traditional EIT method as it has considerably lower computational complexity with sufficient resolving power. This makes it possible to use the proposed EIT method for continuous rapid monitoring of surface cracks during the operation of a controlled construction in real-time mode. The main stages of the proposed modified EIT method, a block diagram of the crack image reconstruction algorithm and a method for processing the crack images, which provide the possibility for adjusting the sensitivity of the monitoring system, are considered. The main modules of the monitoring system software are described. Analysis of the imitative modeling results of the cracks registering processes as a function of size, shape, and the arrangement of cracks, the number of boundary contacts of the distributed sensor, the step of the grid, and the parameters of a digital filter are considered. Comparative analysis of the developed and standard EIT methods for surface cracks monitoring in constructive elements was performed.

Keywords: sensor; surface cracks monitoring; electrical impedance tomography

1. Introduction

Monitoring of cracks occurring in highly loaded structural elements during their operation plays a key role in ensuring the safety and reliability of technical facilities. The hulls of aircraft and ships, the elements of bridges, cranes, and drilling rigs, etc. are subjected to significant mechanical stresses during their operation, initiating the formation and growth of fatigue cracks, which can lead to the destruction of constructions and associated risk for human health and life [1,2]. Therefore, especially relevant are research and development in the field of creating systems of monitoring the integrity of structural elements in the mode of their operation in real-time.

To solve this problem electromagnetic, ultrasonic, optical, radiographic, thermal, electrical methods and other methods are used [3–8]. However, none of the above-listed cracks monitoring methods can be described as universal. For instance, the electromagnetic and ultrasonic methods can be effective under stationary conditions, nevertheless, they cannot be used to monitor the cracks of mobile objects in real-time mode. The piezoelectric and the electrical sensor systems, which are based on film conductors, are convenient for cracks registration in mobile objects while they are operating.

However, they can provide only selective monitoring of the surface being analyzed. For example, the distributed sensor (a system of mutually orthogonal film conductors deposited on a polymer dielectric film, which has been located on a controlled surface) reported in [8] can provide short-term cracks registration, which is sufficient for monitoring the integrity of construction during its operation in real-time mode. As a consequence, minimization of the registered crack dimension, in this case, requires an increase in the number of film conductors. Correspondingly, one should increase the number of contacts, which in turn makes the signal processing system of the sensor more complicated. This means that an important topic is to provide continuous control of the occurrence of cracks and their evolution in certain critical areas of the surface of structural elements using a monitoring system with a small number of sensor contacts.

Continuous monitoring of cracks on areas of interest on construction surfaces can be provided using a distributed sensor. This consists of a conductive film with a given specific conductivity, which completely covers the monitored surface and has electrical contacts located along the perimeter [9–18]. In case the material of the test object has a high conductivity (for example, metal or metal alloy), a sensor film is applied to the dielectric layer present on the monitored surface [7,8]. When the tensile strength limit of the sensor film, which is determined by its thickness, material, and method of deposition is achieved, cracks will appear in it, which are approximately the same in shape, size, and location as the cracks in the monitoring object. Registration and monitoring of cracks in the sensor film can be performed using the method of electrical impedance tomography (EIT) [9–20].

Measurements are carried out with the help of the boundary contacts of the film. A current is passed through two contacts, called current contacts. The remaining (measuring) contacts are used for the voltages measurement. The implementation of the EIT consists of obtaining a large number of measurements for various combinations of current contacts and performing for each measurement, the iterative procedures of numerical solutions of the forward and inverse EIT problems [9–18].

The forward problem of EIT consists of finding the spatial distribution of the potential in the sensor film for the spatial distribution of the film specific conductivity. The most accurate model of the forward problem is the complete electrode model (CEM). The CEM takes into account the boundary contact resistances. The CEM consists of the Laplace Equation (1), boundary conditions (2)–(4), and additional condition (5) [10]:

$$\nabla(\sigma \cdot \nabla \varphi) = 0; \tag{1}$$

$$\varphi + z_c \sigma \cdot \partial \varphi / \partial \boldsymbol{n} = U_c; \tag{2}$$

$$\sigma \cdot \partial \varphi / \partial \boldsymbol{n} = 0; \tag{3}$$

$$\int \sigma \cdot (\partial \varphi / \partial \boldsymbol{n}) \mathrm{d} S_c = I_c; \tag{4}$$

$$\Sigma I_c = 0, \tag{5}$$

where σ is the specific conductivity of the sensor film; φ is the electrostatic potential; I_c is the current passed through the current contact; U_c is the voltage on the c-th boundary contact; S_c is the cross-sectional area of the current contact; $\boldsymbol{n}$ is an outward-pointing normal to the boundary; z_c is the contact impedance between c-th contact and the sensor film.

Equation (4) is the boundary condition for current contacts. Equation (2) is the boundary condition for measuring contacts. It takes into account the contact impedance contribution to the contact potential. Equation (3) is the Neumann condition on the contact-free boundaries of the sensor film. Additional conditions (5) reflect the charge conservation. They also need to be satisfied [10].

The EIT inverse problem iteratively minimizes the difference between a vector of experimentally measured boundary voltages $\boldsymbol{U_m}$ and the vector of boundary voltages $\boldsymbol{F(\sigma)}$ predicted by the forward problem (1)–(5) solution. This minimization can be described by expression (6) [9].

$$\sigma^* = \arg\min_{\sigma}(||\boldsymbol{U_m} - \boldsymbol{F(\sigma)}||^2), \tag{6}$$

where σ* is a vector of the specific conductivity distribution that satisfies the minimization.

The $F(\sigma)$ is defined as a result of linearization performed by a Taylor series expansion on the initial specific conductivity $\sigma^{(0)}$ according to expressions (7)–(9) [9]:

$$F(\sigma) \approx F(\sigma^{(0)}) + J \cdot \Delta\sigma; \tag{7}$$

$$J = \partial F(\sigma^{(0)}) / \partial\sigma; \tag{8}$$

$$\Delta\sigma = \sigma - \sigma^{(0)}, \tag{9}$$

where J is a sensitivity matrix and $\Delta\sigma$ is the matrix of conductivity increments.

The matrix $\Delta\sigma$ is defined by the Tikhonov regularization procedure because J is severely rank-deficient. The specific conductivity distribution is updated iteratively according to expression (10) until the error is sufficiently minimized [9]:

$$\sigma^{(k+1)} = \sigma^{(k)} + \Delta\sigma, \tag{10}$$

where k is the iteration number.

The EIT is well-known and effective method for defect diagnostics. At the same time, the reconstruction problem in EIT is an ill-posed inverse problem, in the sense that the solution is not unique and it is extremely sensitive to measurement noise and modeling errors [10]. The number of boundary contacts, and their size and shape exert a significant influence on the accuracy of the method. As a result, to ensure the required accuracy, it is necessary to increase the number of contacts and the number of grid nodes. This leads to a corresponding increase in the dimension of the EIT problem and, in combination with the iterative character of the numerical solution of the forward and inverse problems, significantly increases the simulation time and increases the requirements for computational resources [15]. In addition, the number of iterations (1)–(10) can change significantly with the size and localization of the cracks, which is an additional problem for registering and monitoring of cracks in the operating mode of the testing object using EIT in real-time.

These disadvantages of cracks detection using EIT were widely investigated and analyzed in [10,11]. In these works, quantitative as well as qualitative crack image EIT-reconstructions were considered. The qualitative difference imaging of cracks reconstruction, as a result of global linearization, is useful when the objective is only to detect and locate cracks. The difference imaging is performed using two sets of EIT measurements. The First is a reference measurement on the defect-free sensor film, and second one is a measurement after cracking. This approach avoids high computational complexity but gives only an approximate qualitative measure of the size and location of the crack. In addition, unwanted artifacts may appear on the image [10,11].

In contrast to the difference imaging, so-called absolute imaging of cracks do not use global linearization. Therefor absolute imaging is a quantitative method for crack image reconstruction. This needs a very computationally expensive iterative solution for a nonlinear inverse problem [10,11].

It should also be noted that in many cases of cracks monitoring in real-time (for example, in the case of aircraft in flight), reducing the time of crack registration is much more important than highly accurate determination of size, shape, and location.

This work is devoted to solving the aforementioned problems by means of development and investigation of a simplified EIT method, and its software implementation for continuous control (registration and monitoring) of surface cracks in real-time. In comparison with the standard EIT methods described in [9–18], the proposed method excludes iterations and the regularization procedure. An accuracy reduction connected with this feature is partially compensated for by a proposed method of digital filtration of cracks images.

2. Modified Method of Surface Cracks Registration and Monitoring

When using electrical impedance tomography for cracks detection, it is important to determine only the relative changes in the conductivity of the sensor film. This opens opportunities for simplification of cracks detection methods and algorithms.

In this work, to solve the problems of electrical impedance tomography listed above, a modified EIT method has been developed. This method does not require iterative procedures. It is significantly less sensitive to the number of measuring contacts and to the step of the grid.

The proposed method provides for periodic measurement of the relative changes in the conductivity of the sensor film between all pairs of contacts located along the perimeter of the film. To do this, the measured conductivity values are normalized by the conductivity values of the initial defect-free film between the corresponding pairs of contacts stored in the system memory.

When measuring the conductivity between any pair of contacts, the density of the measuring current is distributed unevenly throughout the entire volume of the sensor film. In order to simplify the algorithm of cracks detection, we propose to introduce, as an approximation, "conditional conduction channels" (CCC) of a given width between pairs of contacts of the sensor film. This approximation introduces the assumption that the entire measuring current flows inside the corresponding CCC with a uniform distribution of current density over the cross-section of the CCC.

The essence of the proposed method of reconstruction of the images of cracks is to determine for each node of the grid, a relative change in the conductivity of the sensor film averaged over the number of CCCs into which this node enters, which follows the digital filtration of the resulting image. In contrast with the standard EIT method, these procedures exclude the sensitivity matrix and iterative calculations. Therefore regularization is also not required.

The developed method provides for the following main stages:

- Formation of the initial conductivity matrix named *MCI* by measuring the conductivity between all pairs of contacts along the perimeter of a defect-free sensor film. The dimension of the *MCI* matrix is $N_C - 1 \times N_C - 1$, where N_C is a total number of boundary contacts. The element of the m-th row and the n-th column of the *MCI* matrix is equal to the conductivity measured between the m-th and n-th contacts. The *MCI* matrix is formed once at the calibration stage of the monitoring system, and stored in the system memory;

- Formation of the normalized matrix of film conductivity named MCN during registration and monitoring of cracks. The dimension of the MCN matrix is equal to the dimension of MCI. The element of the m-th row and the n-th column of the MCN matrix is defined as the result from dividing the conductivity of the sensor film measured between the m-th and n-th contacts in the monitoring process by the value of the element of the m-th row and the n-th column of the MCI matrix. The MCN matrix is redefined with the frequency specified by the requirements for the parameters of the monitoring system;

- Reconstruction of the image of cracks using the normalized *MCN* matrix of conductivity of film on a two-dimensional rectangular grid:

$$R = \{(x_i, y_j) \mid i = 1, 2, \ldots, I; j = 1, 2, \ldots, J\}, \tag{11}$$

where i, j are the grid nodes indexes; x_i, y_j are the grid nodes coordinates; I is the number of grid nodes along the x coordinate; J is the number of grid nodes along the y coordinate;

- Digital filtering of cracks images in order to adjust the sensitivity threshold of the monitoring system and optimize the contrast of the recorded image.

The developed algorithm for reconstructing the image of cracks (stage 3 of the modified EIT method) is illustrated by the block diagram shown in Figure 1 and a schematic representation of a sensor film with 12 contacts (C_1–C_{12}) along the perimeter, shown in Figure 2.
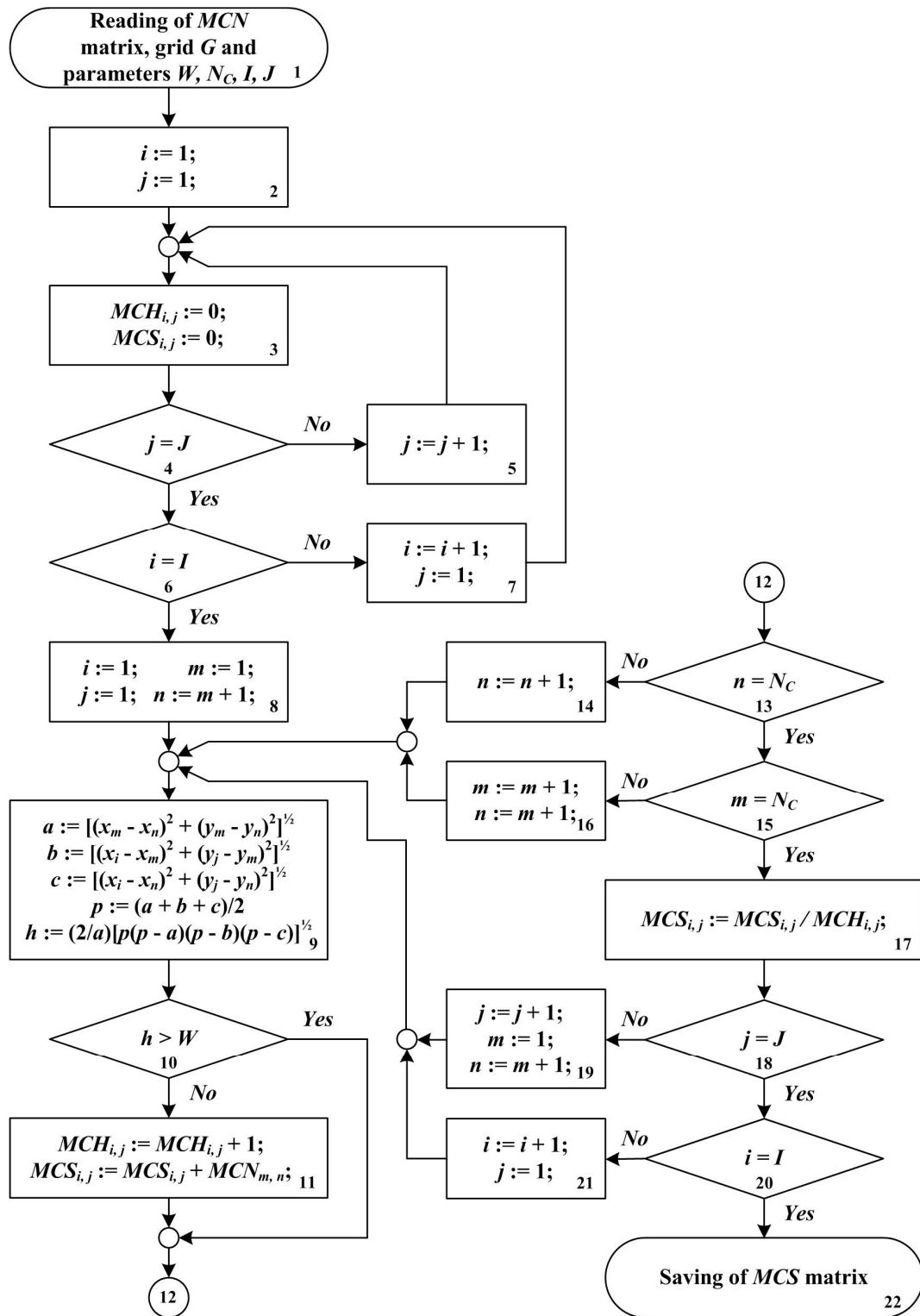
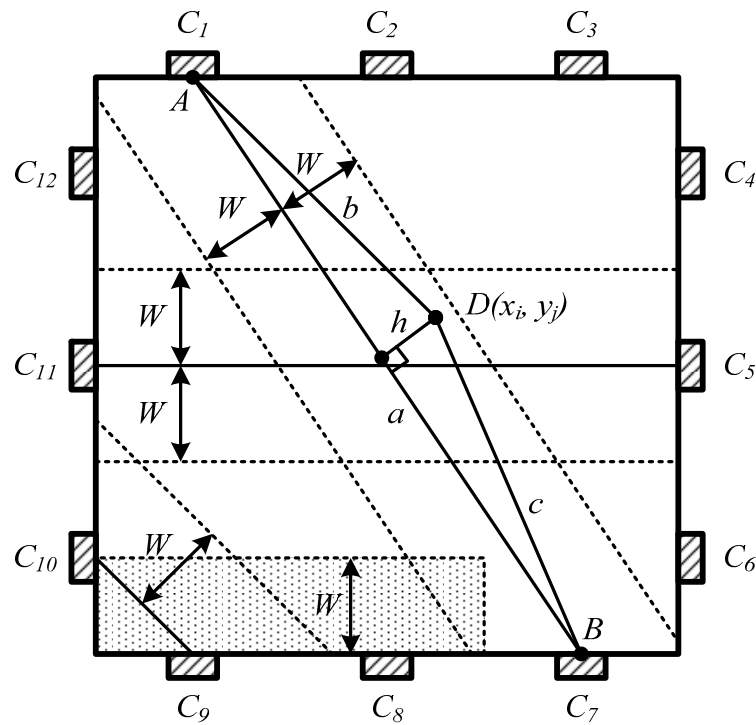**Figure 1.** Block diagram of algorithm for image reconstruction of cracks.

Figure 2. Schematic representation of a sensor film with twelve contacts C_1–C_{12}. Dotted lines show the boundaries of conditional conduction channels with a width of $2W$ between pairs of contacts.

The result of the cracks image reconstruction is the determination of the spatial distribution of the relative specific conductivity of the sensor film averaged over the number of CCC for each node of grid in the form of matrix named *MCS* with a dimension corresponding to the dimension of the coordinate grid R (11). Reconstruction of the image of cracks is performed using the normalized matrix of conductivity *MCN* on the grid R and includes the following procedures:

- Loading of the normalized matrix of conductivity *MCN*, grid R and parameter values W, N_C, I, J (block 1 in Figure 1), where W is the half-width of the "conditional conduction channel" (Figure 2). Between adjacent contacts, the width of the CCC is assumed to be W; for example, between the contacts C_8 and C_9 in Figure 2. The parameter W is a tuning parameter. In the proposed method, the parameter W is a constant for all pairs of boundary contacts, including adjacent contacts. The minimum value of W is determined by the requirement that there are no nodes of the coordinate grid (x_i, y_j) that are not included in any CCC. Consequently in this case, W is defined by the sensor film size and the number of boundary contacts. However, the other versions of the proposed method with dependence on the W parameter on the distances between boundary contacts will be considered in following works;
- Formation of a matrix of conditional conduction channels named *MCH* and a matrix of averaged normalized values of the conductivity named *MCS* of dimension $I \times J$ corresponding to the dimension of the coordinate grid R, with zero elements (blocks 2–7 in Figure 1);
- Sequential execution for all nodes of the grid (x_i, y_j) in the following procedures:

1. Determination of the total number of CCCs, which include the node (x_i, y_j), and assigning this value to the element of the *i*-th row and the *j*-th column of the *MCH* matrix (blocks 8–16 in Figure 1). The implementation of this procedure is shown in Figure 2 by the example of determining the belonging of the point $D(x_i, y_j)$ to the conditional conduction channel between the contacts C_1 and C_7. For this purpose, a triangle ABD with vertices A and B at the central points of contacts C_1 and C_7 is constructed. The height h, dropped to the side AB

from the vertex D is determined in accordance with the expressions presented in block 9 in Figure 1, where a, b, and c are the length of the sides of triangle ABD, and p is half of the triangle ABD perimeter. If $h \leq W$ then node (x_i, y_j) is included in the corresponding CCC and the value of element $MCH_{i,j}$ is incremented by 1 (blocks 10 and 11 in Figure 1);

2. Determination of the element value of the i-th row and the j-th column of the matrix of averaged normalized values of the conductivity MCS (blocks 8–20 in Figure 1) by summing the elements of the normalized matrix of conductivity of the film MCN with the indexes m, n corresponding to the pairs of contacts whose CCCs include the (x_i, y_j) node (block 11 in Figure 1), and then dividing the sum by the element value of the i-th row and the j-th column of the MCH matrix (block 17 in Figure 1);

- Storing and transferring the matrix of averaged normalized values of specific conductivity MCS to a block of cracks images with digital filtering in order to optimize the contrast of the registered image (block 22 in Figure 1). Digital filtration of cracks images was performed in accordance with expressions (12) and (13):

$$MCF_{i,j} = MCS_{i,j} + \gamma \cdot (MCS_{i,j} - CN_{TH}); \tag{12}$$

$$CN_{TH} = \min(MCS) + K_F \cdot [1 - \min(MCS)], \tag{13}$$

where $MCS_{i,j}$ is the element of the i-th row and j-th column of the matrix of average normalized values of specific conductivity; CN_{TH} is a threshold normalized value of specific conductivity; γ, and K_F are the digital filter coefficients; $MCF_{i,j}$ is an element of the i-th row and the j-th column of the matrix named MCF from the results of digital filtering.

The elements of the matrix of averaged normalized values of the specific conductivity $MCS_{i,j}$ satisfy the condition (14).

$$0 \leq MCS_{i,j} \leq 1. \tag{14}$$

The elements of the digital filtering results matrix $MCF_{i,j}$ must also satisfy condition (14). Therefore, if condition (14) in the filtering process is violated, the values of $MCF_{i,j}$ are restricted as follows:

$$\text{if } MCF_{i,j} < 0, \Rightarrow MCF_{i,j} = 0; \tag{15}$$

$$\text{if } MCF_{i,j} > 1, \Rightarrow MCF_{i,j} = 1. \tag{16}$$

The filter coefficient K_F in expression (13) determines the threshold normalized value of the specific conductivity. It is selected in the range:

$$0 < K_F < 1. \tag{17}$$

The filter coefficient γ in expression (12) determines the depth of contrast of the result of digital filtering. The coefficients γ and K_F allow the filter to be adjusted to be the most efficient display of cracks with sizes corresponding to a specified range of values, and thus to adjust the sensitivity of the monitoring system.

3. Imitative Modeling Software Package

To investigate the effectiveness of the proposed modified method of registration and monitoring surface cracks, an imitative modeling software package was developed [21]. This software package includes a software implementation of the cracks image reconstruction algorithm presented in details in Figure 1 and the digital filter described by expressions (12)–(17), as well as a software module of generating the MCI and MCN conductivity matrices and imitating cracks in the sensor film.

The software module of generating the MCI and MCN conductivity matrices and imitating cracks in the sensor film implements the following procedures:

- Recording of the nodal values of the defect-free sensor film specific conductivity $\sigma_{i,j}$ in the matrix *MCI*. Initial spatial distribution of the specific conductivity may be defined as uniform to imitate an ideal sensor film or as random given fluctuations of the conductivity to imitate a real film;
- Imitation of cracks by setting low values of specific conductivity $\sigma_{i,j}$ in certain grid nodes (x_i, y_j) according to the necessary form and size of the crack;
- Numerical solution of the finite-difference representation (18) of the Laplace Equation (1) on the two-dimensional rectangular grid (11) for the sensor film without defects, as well as for the sensor film with cracks:

$$
\begin{aligned}
&[(\sigma_{i+1,j} + \sigma_{i,j})\cdot(\varphi_{i+1,j} - \varphi_{i,j}) - (\sigma_{i,j} + \sigma_{i-1,j})\cdot(\varphi_{i,j} - \varphi_{i-1,j})]/(2\cdot h_x{}^2) + \\
&+ [(\sigma_{i,j+1} + \sigma_{i,j})\cdot(\varphi_{i,j+1} - \varphi_{i,j}) - (\sigma_{i,j} + \sigma_{i,j-1})\cdot(\varphi_{i,j} - \varphi_{i,j-1})]/(2\cdot h_y{}^2) = 0, \\
&i = 2, 3, \ldots, I\text{ - }1; \qquad j = 2, 3, \ldots, J-1,
\end{aligned}
\tag{18}
$$

where i, j are the node indexes excluding boundary nodes; $\sigma_{i,j}$, $\sigma_{i+1,j}$, $\sigma_{i-1,j}$, $\sigma_{i,j+1}$, $\sigma_{i,j-1}$ are the nodal values of the sensor film specific conductivity; $\varphi_{i,j}$, $\varphi_{i+1,j}$, $\varphi_{i-1,j}$, $\varphi_{i,j+1}$, $\varphi_{i,j-1}$ are the nodal values of the electrostatic potential; h_x is a grid step along the direction x; h_y is a grid step along the direction y. For the contacts C_m and C_n, between which the conductivity is measured, the Dirichlet boundary conditions (19) are used:

$$
\varphi_{i,j} = U_{m,n},
\tag{19}
$$

where $U_{m,n}$ is the voltage between contacts C_m and C_n. For the remaining boundaries of the sensor film the finite-difference representation (20) of the Neumann boundary conditions (3) are used:

$$
\begin{aligned}
&(\varphi_{2,j} - \varphi_{1,j})/h_x = 0; \\
&(\varphi_{I,j} - \varphi_{I-1,j})/h_x = 0; \\
&(\varphi_{i,2} - \varphi_{i,1})/h_y = 0; \\
&(\varphi_{i,J} - \varphi_{i,J-1})/h_y = 0;
\end{aligned}
\tag{20}
$$

- Calculation of the spatial distributions of the normal component of current density j_C on the boundaries of contacts C_m and C_n for the sensor film without defects, as well as for the sensor film with cracks using expressions (21) for the different locations of the contacts:

$$
\begin{aligned}
&j_{C1,j} = \sigma_{1,j}\cdot(\varphi_{2,j} - \varphi_{1,j})/h_x; \\
&j_{CI,j} = \sigma_{I,j}\cdot(\varphi_{I,j} - \varphi_{I-1,j})/h_x; \\
&j_{Ci,1} = \sigma_{i,1}\cdot(\varphi_{i,2} - \varphi_{i,1})/h_y; \\
&j_{Ci,J} = \sigma_{i,J}\cdot(\varphi_{i,J} - \varphi_{i,J-1})/h_y;
\end{aligned}
\tag{21}
$$

- Calculation of the currents I_{Cm} and I_{Cn}, flowing through the contacts C_m and C_n, between which the conductivity of the sensor film without cracks is measured by numerical integration of the normal component of the current density over the area of the contacts. Verification of the condition (22):

$$
I_{Cm} + I_{Cn} = 0;
\tag{22}
$$

- Calculation of the currents J_{Cm} and J_{Cn}, flowing through the contacts C_m and C_n, between which the conductivity of the sensor film with cracks is measured, by numerical integration of the normal component of current density over the area of the contacts. Verification of the condition (23):

$$
J_{Cm} + J_{Cn} = 0;
\tag{23}
$$

- Assignment to the element of the *m*-th row and the *n*-th column of the matrix *MCI* of the conductivity value $G_{m,n}$ between the contacts C_m and C_n for the film without cracks, determined by the expression (24):

$$MCI_{m,n} = G_{m,n} = |I_{Cm}|/U_{m,n}; \tag{24}$$

- Assignment to the element of the *m*-th row and the *n*-th column of the matrix *MCN* of the conductivity value between the contacts C_m and C_n for the film with cracks normalized by the $MCI_{m,n}$, determined by the expression (25):

$$MCN_{m,n} = (|J_{Cm}|/U_{m,n})/MCI_{m,n}. \tag{25}$$

4. Results of Imitative Modeling and Discussion

In the process of the study of the effectiveness of the proposed modified method of surface cracks registration and monitoring using a software package [21], the results of imitative modeling were obtained by varying the following parameters:

- Number of contacts to the sensor film;
- Number of grid nodes;
- Digital filter parameters;
- Size of cracks;
- Location of cracks;
- Specific conductivity of the initial (defect-free) sensor film.

The results of imitative modeling of the crack detection process, obtained by the number of grid nodes 73 × 73 for 8, 12, 16, 20, and 24 boundary contacts, are shown in Figure 3.

The results of imitative modeling of the crack detection process, obtained for 12 boundary contacts and for the number of grid nodes 31 × 31, 79 × 79, 103 × 103, are shown in Figure 4.

The results in Figures 3 and 4 were obtained at the parameters of the digital filter $\gamma = 1 \times 10^4$, $K_F = 0.03$ for the manganin sensor film with a specific conductivity of 2.33×10^6 S/m.

The imitative modeling results presented in Figures 3 and 4 showed that at the number of contacts of 12 and more, the increase in the number of contacts and the number of grid nodes practically did not affect the detection efficiency of cracks and the quality of their images. Only at a number of contacts of less than 12 was there is a significant decrease in the cracks image quality. The properties of the proposed method provided a significant reduction in the required hardware resources and computational complexity when implemented in comparison with the standard EIT method.

The results of the imitative modeling of the process of registering the crack shown in Figure 4a, obtained at the number of grid nodes 103 × 103 for the 12 boundary contacts and for the parameters of the digital filter $\gamma = 1 \times 10^4$, $K_F = 0.03$–0.09 are shown in Figure 5.

As shown above, the essence of the proposed method of reconstruction of the images of cracks was to determine for each node of the grid, a relative change in the conductivity of the sensor film averaged over the number of "conditional conduction channels", into which this node entered. In contrast with the standard EIT method, these procedures excluded the sensitivity matrix and iterative calculations. Therefore, regularization was also not required. Obviously, this led not only to a minimization of the complexity and time for the calculations, but to some reduction in the accuracy of the proposed method in comparison with the standard EIT. This accuracy reduction was partially compensated by the proposed method of digital filtration of the cracks images.

Confirmation of the acceptability and efficiency of the CCC approximation with the uniform spatial distribution of the current density were the results of imitative modeling, as shown in Figures 3–8. However, another version of the proposed method with some more realistic approximations of the uneven distributions of the current density in the CCCs will be considered in future works.

The results presented in Figure 5 show that the change in the K_F parameter of the digital filter had a significant effect on the image quality of the registered crack, and allows tuning of the cracks monitoring system to a specified minimum size of the crack. It is important to note that such tuning can be carried out in the mode of the system operation according to a certain algorithm developed in accordance with the requirements for the operating conditions of the monitoring object.
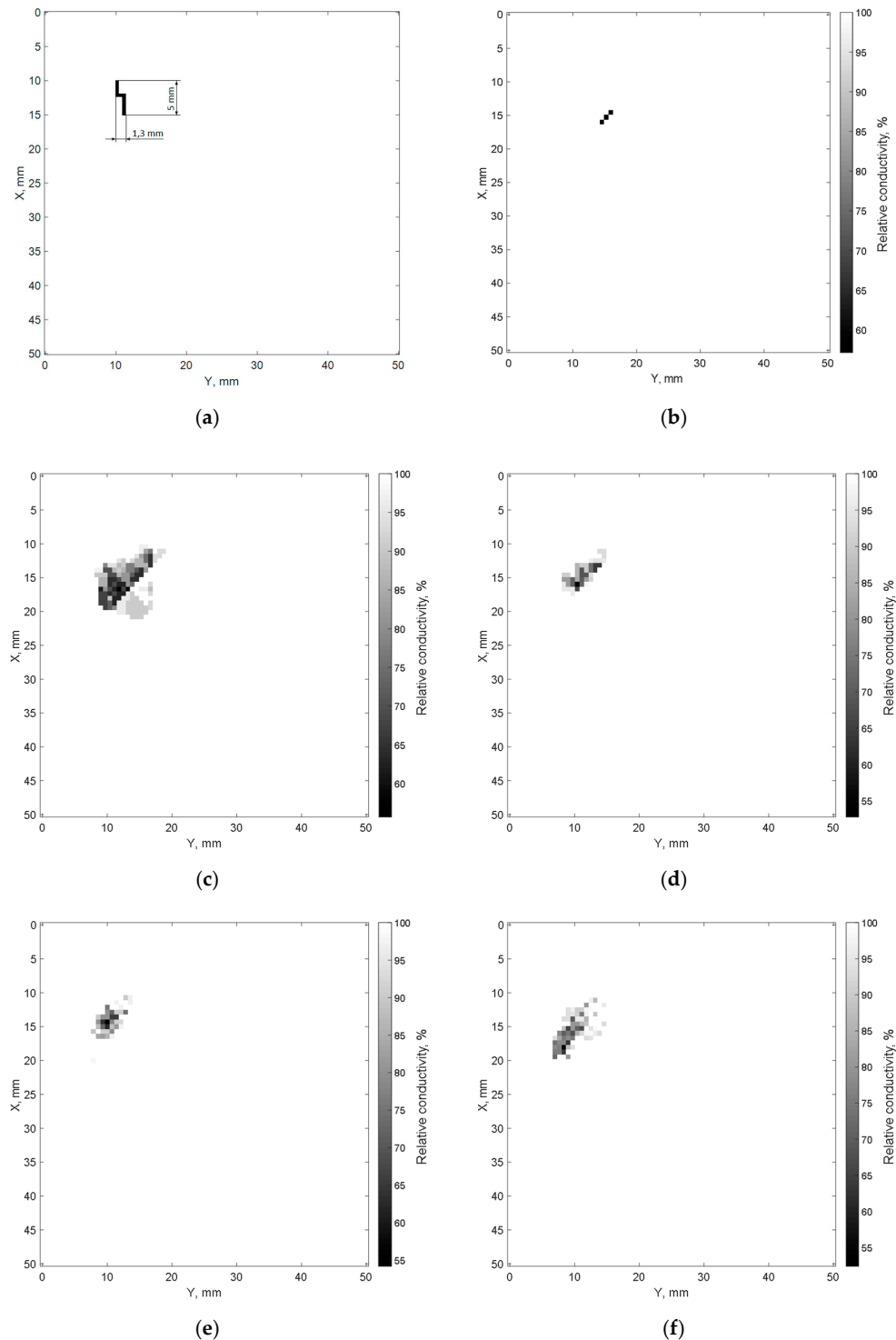
Figure 3. Results of imitative modeling of the crack (**a**) detection process obtained at a specific conductivity of the initial sensor film of 2.33×10^6 S/m, with a grid node number of 73×73, for the parameters of the digital filter $\gamma = 1 \times 10^4$, $K_F = 0.03$ for 8 (**b**), 12 (**c**), 16 (**d**), 20 (**e**), and 24 (**f**) contacts.
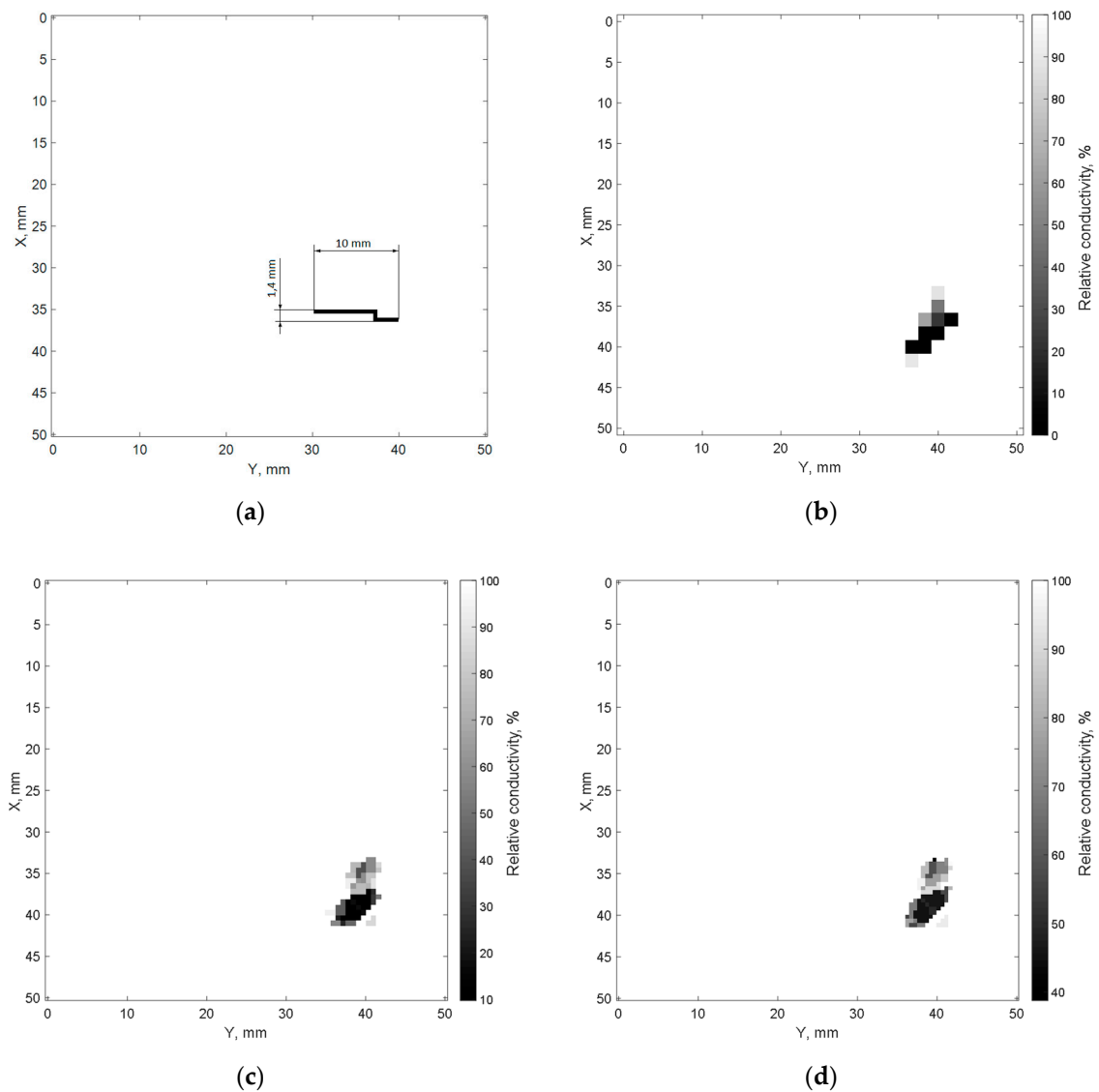
Figure 4. Results of imitative modeling of the process of the crack (**a**) detection obtained at a specific conductivity of the initial sensor film at 2.33×10^6 S/m, for the 12 contacts, with the digital filter parameters $\gamma = 1 \times 10^4$ and $K_F = 0.03$ for the coordinate grids with a node number of 31×31 (**b**), 79×79 (**c**), 103×103 (**d**).

The results of imitative modeling of the process of cracks detection, obtained for the 16 boundary contacts and the parameters of the digital filter $\gamma = 1 \times 10^4$, $K_F = 0.05$, for different sizes of cracks and different variants of cracks locations, are shown in Figures 6 and 7 respectively.

The simulation results presented in Figures 6 and 7 demonstrate satisfactory sensitivity of the proposed method to the sizes and spatial localization of the registered cracks at a relatively small number of contacts (more than 12) and a small number of grid nodes (in the considered examples 41×41 and 49×49). In this case, with a certain distortion in the sizes and spatial arrangement of the cracks images, due to the peculiarities of the proposed method, in particular, the absence of iterative procedures in the reconstruction of these images was observed. Figures 6 and 7 show that the observed distortions in the size and spatial arrangement of the cracks were insignificant and permissible for the purpose of diagnostics of the integrity of the technical objects.

The results of imitative modeling of the process of crack registration, obtained for the specific conductivity of the initial sensor film 8.93×10^5 S/m (nichrome), 2.33×10^6 S/m (manganin), and 1.82×10^7 S/m (tungsten), are shown in Figure 8.

The images presented in Figure 8 show that the proposed method of cracks registration and monitoring gave the same results when using conductive sensory films with different conductivity values (in the considered examples 8.93×10^5–1.82×10^7 S/m).

The insensitivity to the specific conductivity of the sensor film material was important for ensuring the reproducibility of the characteristics of the cracks registration and the monitoring systems in the process of their production, and was provided by normalizing the elements of the *MCN* matrix in accordance with expression (25).
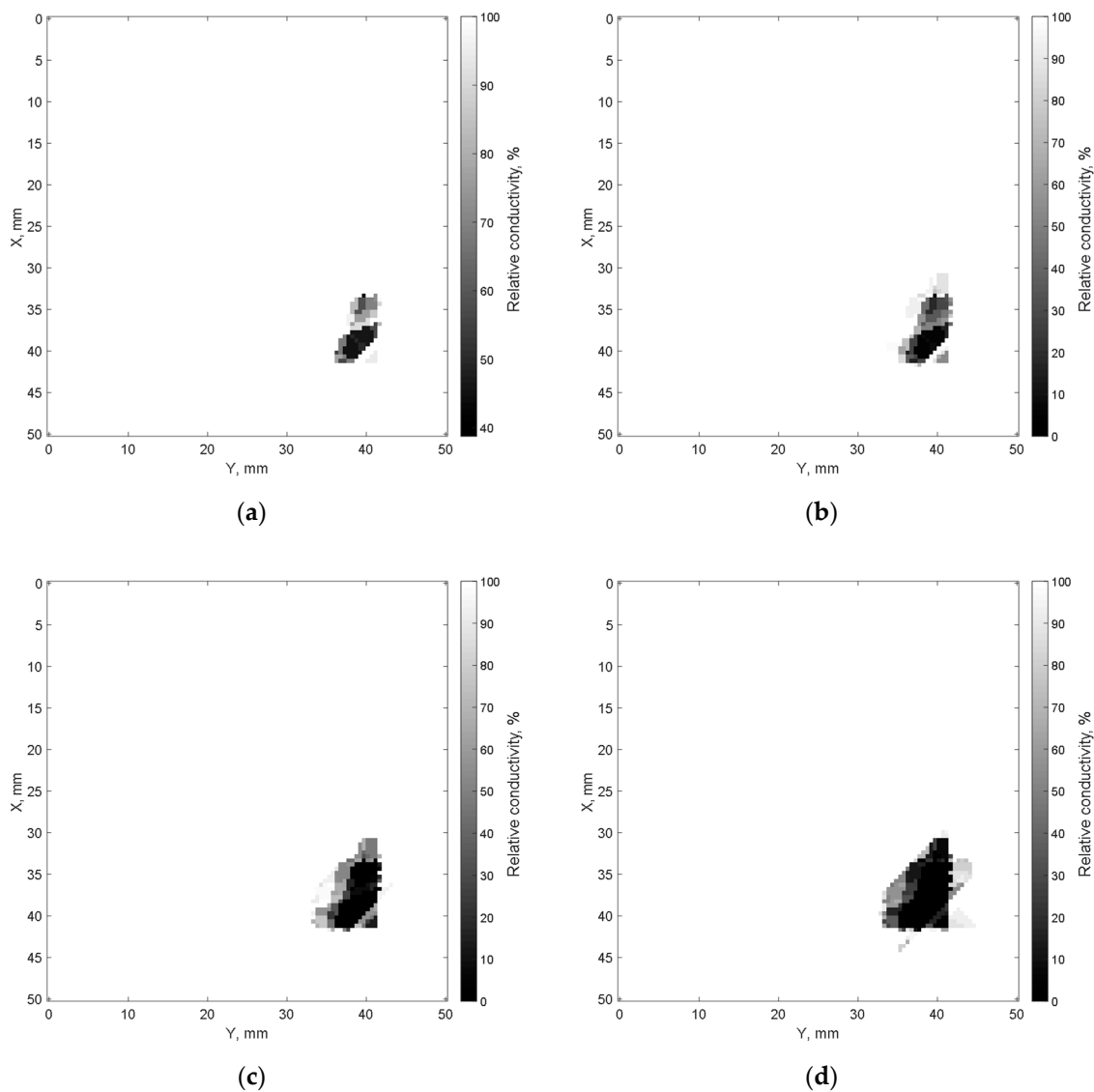
(**a**)

(**b**)

(**c**)

(**d**)

Figure 5. Results of the imitative modeling of the process of registering the crack shown in Figure 4a, obtained at a specific conductivity of the initial sensor film of 2.33×10^6 S/m, with a grid node number of 103×103, for the 12 contacts, for the parameters of the digital filter $\gamma = 1 \times 10^4$, $K_F = 0.03$ (**a**), $K_F = 0.05$ (**b**), $K_F = 0.07$ (**c**), $K_F = 0.09$ (**d**).

This property is also extremely important for ensuring the effective functioning of the monitoring system under the influence of destabilizing factors of the external environment; for example, when the temperature of the controlled surface is changed by several tens of degrees.
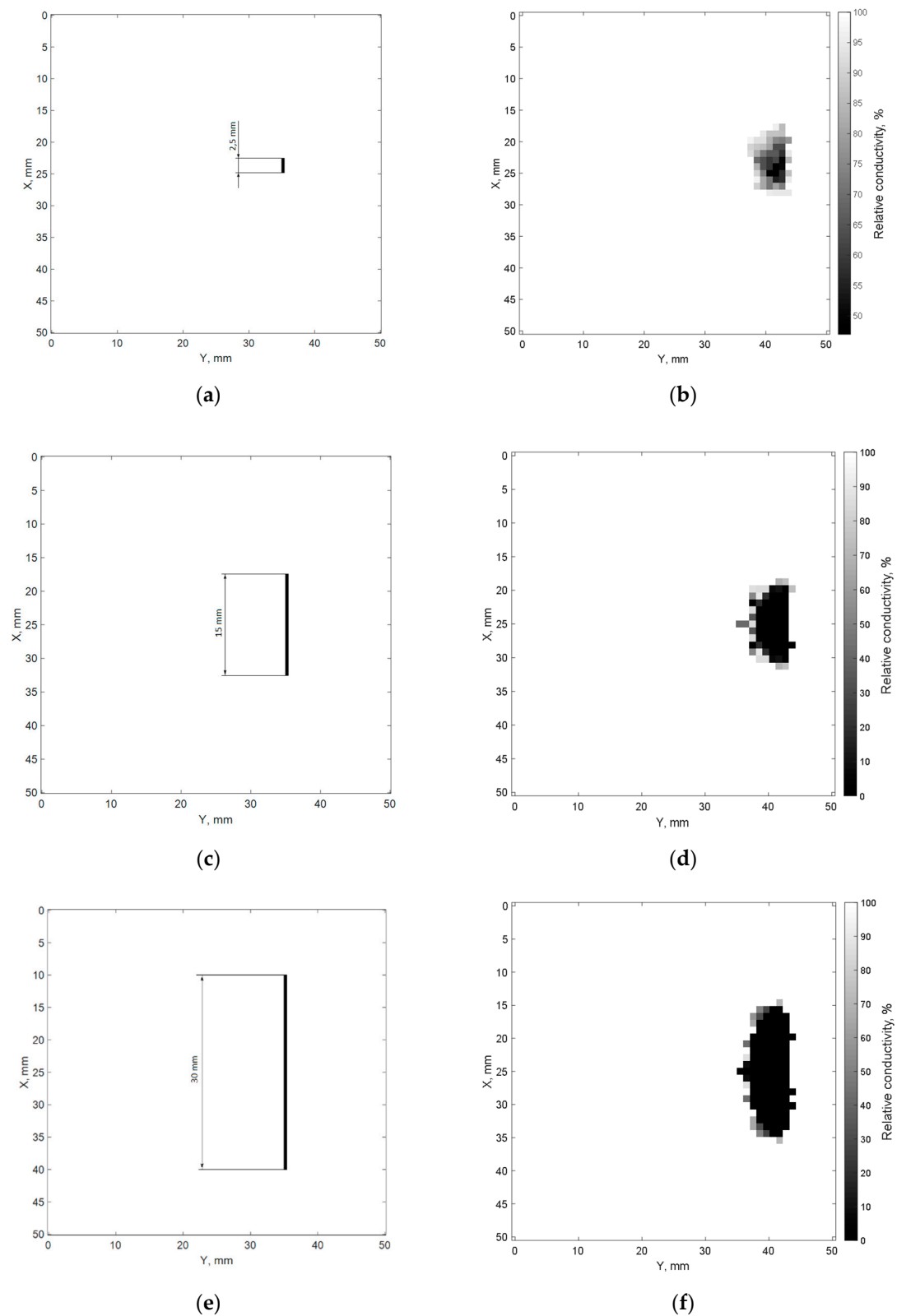
Figure 6. Results of the imitative modeling (**b**), (**d**), (**f**) obtained at a specific conductivity of the initial sensor film of 2.33 × 10⁶ S/m, with a grid node number of 49 × 49, at the parameters of the digital filter γ = 1 × 10⁴, K_F = 0.05, for the 16 contacts, for crack sizes 2.5 mm (**a**), 15 mm (**c**), and 30 mm (**e**).
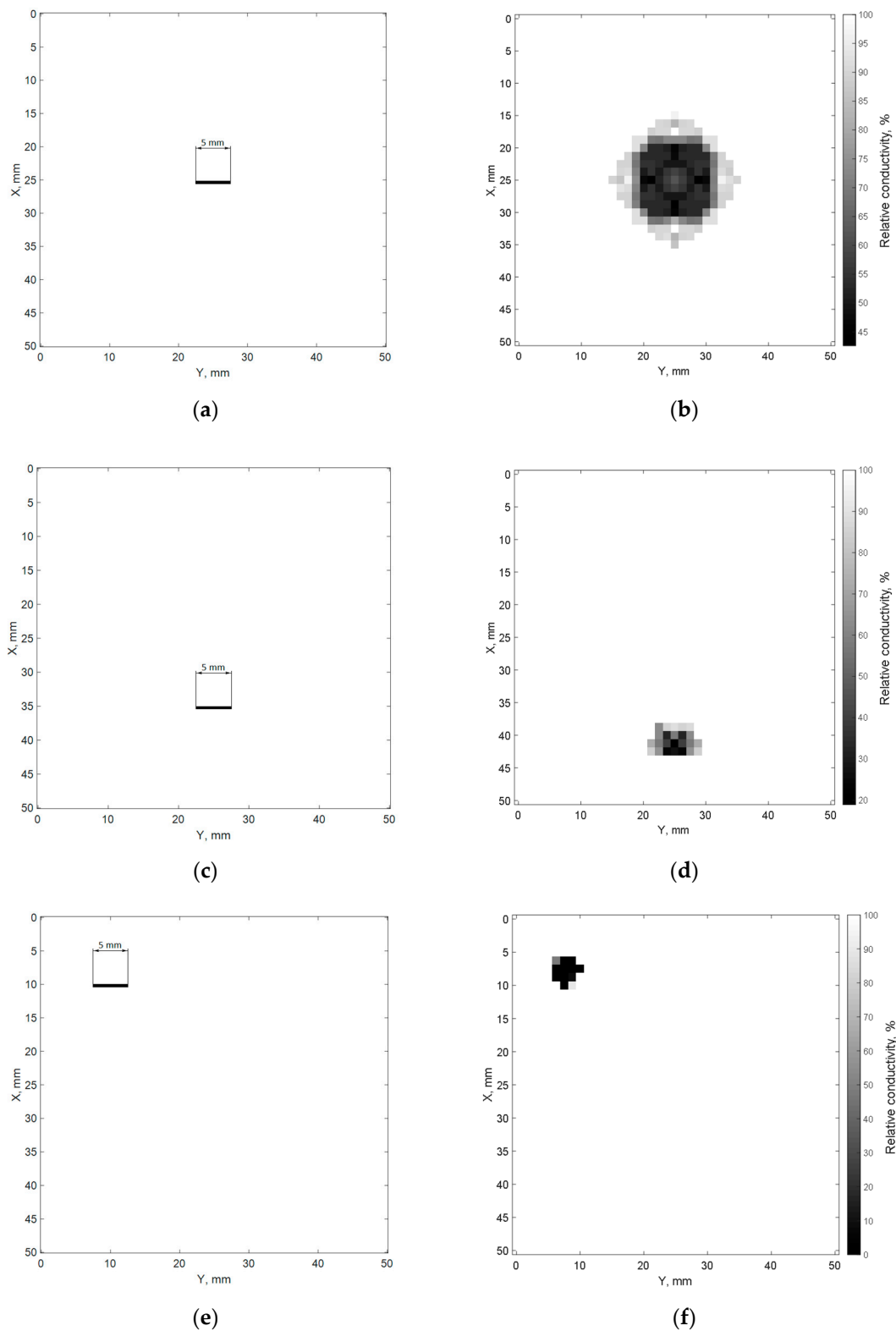
Figure 7. Results of the imitative modeling (**b**), (**d**), (**f**) obtained at a specific conductivity of the initial sensor film of 2.33×10^6 S/m, at a grid node number of 41×41, at the parameters of the digital filter $\gamma = 1 \times 10^4$, $K_F = 0.05$, for the 16 contacts, for different variants of crack location: center (**a**), bottom side (**c**), and upper-left corner (**e**).
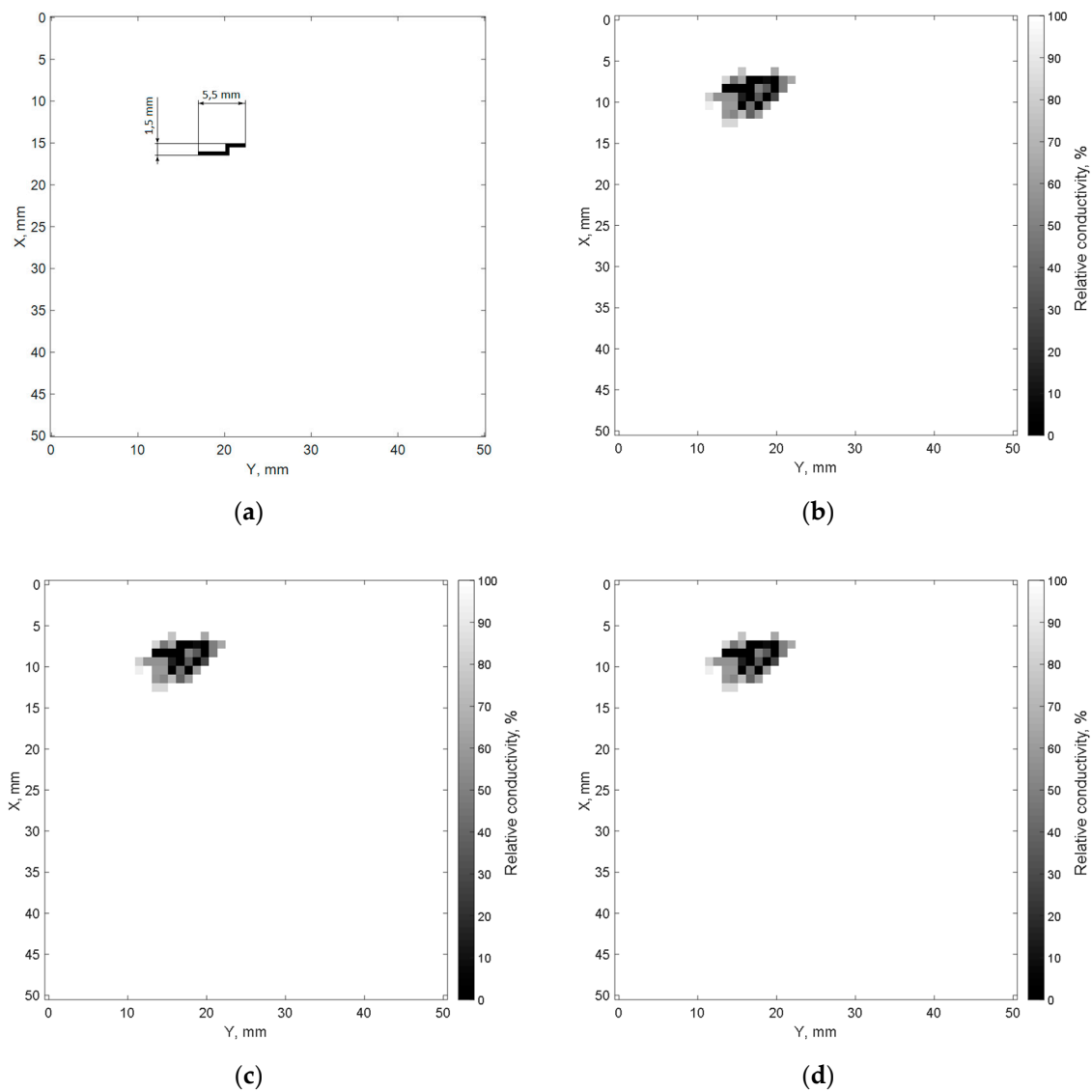
(a)

(b)

(c)

(d)

Figure 8. Results of imitative modeling of the process of crack (**a**) registration, obtained at a grid node number of 49×49, at the digital filter parameters $\gamma = 1 \times 10^4$, $K_F = 0.05$, for the 16 contacts, for the initial sensor film conductivity of 8.93×10^5 S/m (nichrome) (**b**), 2.33×10^6 S/m (manganin) (**c**), and 1.82×10^7 S/m (tungsten) (**d**).

In this case, to extend the operating temperature range, it is necessary to:

- supplement the system of registering and monitoring cracks by the temperature sensor of the sensor film;
- when forming the initial *MCI* conductivity matrix, carry out conductivity measurements between all pairs of contacts along the perimeter of a defect-free sensor film in the entire required temperature range with a certain increment in temperature set in accordance with the required accuracy of determining the size and location of the cracks. The *MCI* matrixes obtained for all temperature values must be stored in the system memory;
- when forming the normalized *MCN* matrix of film conductivity during the registration and monitoring of cracks, perform the normalization in accordance with expression (25) using elements of the *MCI* matrix corresponding to the current temperature sub-band recorded by the temperature sensor.

Because the required number of boundary contacts of the sensor film was small, an increase in the number of *MCI* matrices in accordance with the number of temperature sub-bands did not constitute a technical problem and did not require significant computing resources. A more serious problem was the change in the mechanical properties of the sensor film when the temperature varied over a wide range, which must be taken into account when choosing the film material, and is a separate task.

At the hardware implementation of the proposed method of registering and monitoring of cracks, the conductivity of the sensor film can be measured by one of the well-known methods [22,23]. Taking into account that the measurement of the conductivity of the initial sensor film and the conductivity of the film during the monitoring of cracks is carried out by one method, the procedure (25) of normalizing the *MCN* matrix will help to minimize the effect of systematic error in conductivity measurements on the efficiency of registering and monitoring of cracks.

5. Conclusions

As a result of the performed study, a method of continuous control of surface cracks and monitoring of their growth, based on measuring the changes in conductivity between contacts of the sensor conductive film, which ensures high productivity in the process of cracks detection, has been developed. A method of processing the image of cracks and providing the possibility of adjusting the sensitivity of the monitoring system, has been proposed. An algorithm and software implementation for the developed monitoring method [21] have been considered.

The results of imitative modeling of the surface cracks monitoring system have been obtained. An analysis of simulation results depending on the size, shape, and location of the cracks, on the number of peripheral contacts to the distributed sensor, and on the number of grid nodes determining the resolution and computational complexity of the proposed method, has been performed.

It has been shown that in comparison with the standard EIT methods described in [9–18], the proposed method excludes iterations and regularization procedures. This leads not only to minimization of the complexity and time of calculations, but to some reduction of the accuracy of the proposed method in comparison with the standard EIT. An accuracy reduction connected with this feature is partially compensated for by the proposed method of digital filtration of cracks images.

At the same time, other variants of the proposed method with more realistic approximations of nonuniform current density distributions in "conditional conduction channels", and with the dependence of the CCC width on the distances between boundary contacts, will be considered in the following works.

References and Note

1. Rathod, V.R.; Anand, R.S.; Ashok, A. Comparative analysis of NDE techniques with image processing. *Nondestruct. Test. Eval.* **2012**, *27*, 305–326. [CrossRef]
2. Turnbull, A. Characterising the early stages of crack development in environment-assisted cracking. *Corros. Eng. Sci. Technol.* **2017**, *52*, 533–540. [CrossRef]
3. Robinson, M.J.; Strutt, J.E. On-line monitoring of crack propagation. *Metals Technol.* **1982**, *9*, 251–256. [CrossRef]

4.　Bernasconi, A.; Carboni, M.; Comolli, L.; Galeazzi, R.; Gianneo, A.; Kharshiduzzaman, M. Fatigue crack growth monitoring in composite bonded lap joints by a distributed fiber optic sensing system and comparison with ultrasonic testing. *J. Adhes.* **2016**, *92*, 739–757. [CrossRef]

5.　Muneesh, M.; Annamdas, V.M.G.; Pang, J.L.H.; Asundi, A.; Tjin, S.C. Crack monitoring using multiple smart materials; fiber-optic sensors & piezo sensors. *Int. J. Smart Nano Mater.* **2017**, *8*, 41–55. [CrossRef]

6.　Noethen, M.; Jia, Y.; Meyendorf, N. Simulation of the surface crack detection using inductive heated thermography. *Nondestruct. Test. Eval.* **2012**, *27*, 139–149. [CrossRef]

7.　Isaeva, A.S.; Konoplev, B.G.; Ryndin, E.A. Analysis of a two-dimensional symmetric problem on extension of a Al-polyimide-Cu layered structure with a model crack. *Tech. Phys. Lett.* **2015**, *41*, 599–601. [CrossRef]

8.　Konoplev, B.G.; Ryndin, E.A.; Isaeva, A.S.; Denisenko, M.A. System of Surface Defect Monitoring Based on a Distributed Crack Sensor. *Electronics* **2017**, *81*, 1–7. [CrossRef]

9.　Tallman, T.N.; Gungor, S.; Wang, K.W.; Bakis, C.E. Tactile imaging and distributed strain sensing in highly flexible carbon nanofiber/polyurethane nanocomposites. *Carbon* **2015**, *95*, 485–493. [CrossRef]

10.　Hallaji, M.; Pour-Ghaz, M. A new sensing skin for qualitative damage detection in concrete elements: Rapid difference imaging with electrical resistance tomography. *NDT E Int.* **2014**, *68*, 13–21. [CrossRef]

11.　Hallaji, M.; Seppänen, A.; Pour-Ghaz, M. Electrical impedance tomography-based sensing skin for quantitative imaging of damage in concrete. *Smart Mater Struct.* **2014**, *23*, 085001. [CrossRef]

12.　Tallman, T.N.; Gungor, S.; Wang, K.W.; Bakis, C.E. Damage detection and conductivity evolution in carbon nanofiber epoxy via electrical impedance tomography. *Smart Mater Struct.* **2014**, *23*, 045034. [CrossRef]

13.　Tallman, T.N.; Semperlotti, F.; Wang, K.W. Enhanced delamination detection in multifunctional composites through nanofiller tailoring. *J. Intell. Mater. Syst. Struct.* **2015**, *26*, 2565–2576. [CrossRef]

14.　Tallman, T.N.; Gungor, S.; Wang, K.W.; Bakis, C.E. Damage detection via electrical impedance tomography in glass fiber/epoxy laminates with carbon black filler. *Struct Health Monit.* **2015**, *14*, 100–109. [CrossRef]

15.　Tallman, T.N.; Wang, K.W. Damage and strain identification in multifunctional materials via electrical impedance tomography with constrained sine wave solutions. *Struct Health Monit.* **2016**, *15*, 235–244. [CrossRef]

16.　Saulnier, G.J.; Blue, R.S.; Newell, J.C.; Isaacson, D.; Edic, P.M. Electrical impedance tomography. *IEEE Signal Process Mag.* **2001**, *18*, 31–43. [CrossRef]

17.　Cherepenin, V.A.; Karpov, A.Y.; Korjenevsky, A.V.; Kornienko, V.N.; Kultiasov, Y.S.; Ochapkin, M.B.; Trochanova, O.V.; Meister, J.D. Three-dimensional EIT imaging of breast tissues: system design and clinical testing. *IEEE Trans. Med. Imaging* **2002**, *21*, 662–667. [CrossRef] [PubMed]

18.　Dharap, P.; Li, Z.; Nagarajaiah, S.; Barrera, E.V. Nanotube Film Based on Single-Wall Carbon Nanotubes for Strain Sensing. *Nanotechnology* **2004**, *15*, 379–382. [CrossRef]

19.　Hou, T.; Loh, K.J.; Lynch, J.P. Spatial conductivity mapping of carbon nanotube composite thin films by electrical impedance tomography for sensing applications. *Nanotechnology* **2007**, *18*, 1–9. [CrossRef]

20.　Loh, K.J.; Kim, J.; Lynch, J.P.; Kam, N.W.S.; Kotov, N.A. Multifunctional layer-by-layer carbon nanotube-polyelectrolyte thin films for strain and corrosion sensing. *Smart Mater. Struct.* **2007**, *16*, 429–438. [CrossRef]

21.　Ryndin, E.A. Program of defect modeling in a thin conducting film from the results of measuring the conductivity between peripheral contacts. Certificate of the Russian Federation on the state registration of a computer program No. 2017619586, 28 August 2017.

22.　Kuznetsov, E.V. Electrical and magnetic circuits. In *Electrical Technics and Electronics*; Lunin, V.P., Ed.; Yurayt Publishing House: Moscow, Russia, 2017; Volume 1, pp. 19–25, ISBN 978-5-534-00356-7.

23.　Bajda, L.I.; Dobrotvorsky, N.S.; Dushin, E.M.; Ismailov, Sh.Yu.; Mokienko, D.N.; Preobrazhensky, A.A.; Staroseltseva, E.A.; Fremke, L.V.; Tsvetkov, E.I. *Electrical Measurements*; Energiya: Leningrad, Russia, 1980; pp. 144–147.